



Sensitive determination of caffeoylquinic acid in food and blood samples using nanostructured conducting polymer composite modified electrode

Hao Tang^a, Jian Shen^c, Jindong Dai^c, Kanagaraj Rajalakshmi^c, Selvaraj Muthusamy^{c,*}, Palanisamy Kannan^{b,*}, Dongwei Zhu^{c,*}, Benshuai You^{d,*}, Xiaojian Liu^{e,*}

^a Department of Clinical Laboratory, Affiliated People's Hospital of Jiangsu University, 212006 Zhenjiang, Jiangsu, PR China

^b College of Biological, Chemical Sciences and Engineering, Jiaxing University, Jiaxing, Zhejiang 314001, PR China

^c Department of Immunology, Jiangsu Key Laboratory of Laboratory Medicine, School of Medicine, School of Chemistry and Chemical Engineering, Jiangsu University, Zhenjiang 212013, PR China

^d Clinical Laboratory Center, The Affiliated Taizhou People's Hospital of Nanjing Medical University, Taizhou 225300, Jiangsu, PR China

^e Department of Gynecology, Affiliated People's Hospital of Jiangsu University, 212006 Zhenjiang, Jiangsu, PR China

ARTICLE INFO

Keywords:

3-Caffeoylquinic acid
Caffeine
MWCNTs
Polymer composite film
Sensor

ABSTRACT

3-Caffeoylquinic acid (3-CQA), a prominent phenolic acid, plays a critical role in glucose metabolism and is associated with the prevention of type-2 diabetes. The selective and sensitive detection of 3-CQA remains challenging due to interferences from substances such as caffeine (CAF) and the instability of signals from unmodified electrodes. To address this, this study developed a nanostructured conducting polymer composite based on acid-functionalized multi-walled carbon nanotubes (FMWCNTs) and 3-amino-5-mercapto-1,2,4-triazole (AMTa), which was integrated onto a glassy carbon electrode (GCE) for the selective detection of 3-CQA. The composite electrode (GCE/OD/FMWCNTs/p-AMTa) was thoroughly characterized using scanning electron microscopy (SEM), Fourier-transform infrared spectroscopy (FT-IR), atomic force microscopy (AFM), X-ray photoelectron spectroscopy (XPS), and electrochemical analysis. In contrast to the unmodified GCE, which fails to maintain a stable voltametric profile for 3-CQA detection due to the deposition of its oxidation products, the composite-modified electrode demonstrates a stable electrochemical response, with a fourfold increase in the catalytic oxidation current. This improvement is attributed to the strong electrostatic and hydrogen-bonding interactions between the heteroatoms in the polymer backbone of p-AMTa and 3-CQA, as well as the π - π interactions between FMWCNTs and the aromatic ring of 3-CQA. Additionally, selective determination of 3-CQA is achieved even in the presence of 500 times the concentration of CAF. The amperometric *i*-*t* curve exhibits a significant increase in response to 3-CQA concentrations ranging from 0.1 to 200 μ M, with a detection limit (LOD) of 30 nM (*S*/*N* = 3). The proposed sensor demonstrates excellent performance in detecting 3-CQA in blood, coffee, tea, and various food samples, yielding satisfactory recovery results.

1. Introduction

3-Caffeoylquinic acid (3-CQA), chemically identified as [(3,4-dihydroxyphenyl)-prop-2-enoyl]oxy-1,4,5-trihydroxycyclohexane-1-carboxylic acid (Fig. 1), is a hydroxycinnamic acid derivative. This polyphenolic compound is an ester of quinic acid and caffeic acid (de Souza Farias et al., 2021; Tong et al., 2021), and is predominantly found in various plants, including apricots, cherries, strawberries, tomatoes, peaches, plums, apples, pears, blueberries, peanuts, coffee beans, and potatoes (Tong et al., 2021). Like other o-dihydroxyphenols, 3-CQA

exhibits free radical scavenging activity (Agar et al., 2015) and cancer chemopreventive effects. Beyond its inhibitory action against tongue carcinogenesis (Tajik et al., 2017), 3-CQA may mitigate the health risks associated with cardiovascular diseases by reducing the oxidation of low-density lipoprotein cholesterol and modulating glucose-6-phosphatase activity in glucose metabolism (Cho et al., 2010). Zhang et al. (2010) highlighted 3-CQA's potential as a therapeutic agent for treating acute lung injury. Furthermore, it inhibits 8-hydroxy-deoxyguanosine, a well-established marker of oxidative DNA damage and cellular oxidative stress during carcinogenesis (Kasai et al., 2000). Despite its

* Corresponding authors.

E-mail addresses: rajselva311@ujs.edu.cn (S. Muthusamy), ktpkannan@zjxu.edu.cn (P. Kannan), 1000005601@ujs.edu.cn (D. Zhu), youbenshuai@163.com (B. You), jingxiaojingx@163.com (X. Liu).

<https://doi.org/10.1016/j.foodchem.2025.145337>

Received 24 February 2025; Received in revised form 21 June 2025; Accepted 24 June 2025

Available online 25 June 2025

0308-8146/© 2025 Elsevier Ltd. All rights reserved, including those for text and data mining, AI training, and similar technologies.

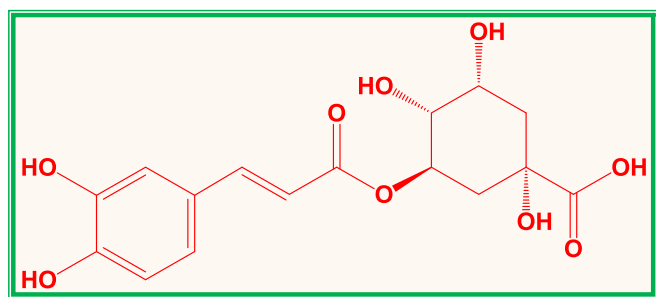


Fig. 1. Chemical structure of 3-CQA.

antioxidant properties, 3-CQA can also induce DNA damage in the presence of transition metals (Duthie et al., 1997), and at high temperatures or in the presence of cupric ions (Yang et al., 2008; Zheng et al., 2008). Plant polyphenols, including 3-CQA, exhibit auto-oxidative behavior, producing reactive oxygen species such as superoxide anions and semiquinone intermediates (Yang et al., 2008). Coffee, being the most widely consumed beverage globally, is the primary dietary source of 3-CQA (Olthof et al., 2001). Clifford (1999) estimated the daily intake of 3-CQA from coffee to be approximately 0.5–1.0 g. Therefore, accurate determination of 3-CQA levels in commercial coffee drinks is of significant health importance.

Numerous techniques have been developed for the detection of 3-CQA, including chemiluminescence (Chen et al., 2021), chromatography (Gigl et al., 2022), high-performance liquid chromatography (Krizman et al., 2007; Zhang et al., 2023), capillary electrophoresis (Xie et al., 2022), and electroanalytical methods (Alagumalai et al., 2022; Mariyappan et al., 2022; Munteanu & Apetrei, 2021). However, compared to electroanalytical methods, other techniques suffer from drawbacks such as high costs, extended operation times, lower sensitivity and selectivity, and more complex procedures. In recent decades, the development of advanced materials for electrochemical detection has seen rapid progress. For instance, MXene-based materials have garnered significant attention due to their tunable surface functional groups and large surface area (Umapathi, Raju, et al., 2025). Similarly, hexagonal boron nitride composite film sensors have been developed for their stability, dielectric properties, and mechanical robustness (Umapathi, Rethinasabapathy, et al., 2025). Carbon nanotube (CNT)/polymer composites have also gained substantial interest in electrochemical sensors because of their synergistic effects, where CNTs contribute excellent electrical conductivity, high surface area, mechanical strength, and efficient electron transport, while polymer films enhance catalytic activity, sensitivity, and molecular recognition.

In light of these advancements, this study aims to fabricate a functionalized multi-walled carbon nanotube (FMWCNT)-3-amino-5-mercapto-1,2,4-triazole (p-AMTa) polymer composite modified glassy carbon electrode (GCE) for the selective and sensitive electrochemical detection of 3-CQA in food and blood samples under physiological conditions. The potentiodynamic polymerization of AMTa on the FMWCNT-modified GCE was utilized to prepare the polymer composite-modified electrode (GCE/OD/FMWCNTs/p-AMTa). The presence of FMWCNTs on the electrode surface facilitates π - π interactions with 3-CQA, increases the surface area, and, together with the p-AMTa, establishes electrostatic and hydrogen-bonding interactions with 3-CQA. These combined effects significantly enhance the sensitivity of the composite-modified GCE toward 3-CQA detection. The polymer composite-modified electrode exhibited a stable voltametric response for 3-CQA detection, with a fourfold increase in oxidation current compared to the unmodified GCE. Amperometric measurements showed a linear increase in catalytic current in response to 3-CQA concentrations ranging from 0.1 to 200 μ M, with a limit of detection (LOD) of 30 nM (S/N = 3). The practicability of the FMWCNTs/p-AMTa composite electrode was demonstrated through the detection of 3-CQA in blood

serum, coffee bean extracts, tea extracts, and various food samples, including potatoes, tomatoes, apples, and grapes, yielding favorable recovery results.

2. Experimental details

2.1. Chemicals

3-Amino-5-mercapto-1,2,4-triazole (AMTa), acid functionalized multi-walled carbon nanotubes (FMWCNTs), dicyclohexylcarbodiimide (DCC), 1,8-octanediamine (OD), caffeine (CAF), and 3-caffeoylquinic acid (3-CQA) were purchased from Merck (Nanjing, Jiangsu, China) and used as received. All other chemicals of analytical grade were also used as received in this study.

2.2. Instrumentations

Electrochemical measurements were conducted using a CHI-634B electrochemical workstation (CHI Instruments, Austin, TX, USA). For standard electrochemical analysis, a mirror-polished GCE (3 mm), platinum wire, and NaCl-saturated Ag/AgCl were employed as the working, counter, and reference electrodes, respectively. During differential pulse voltammetry (DPV) analysis, a pulse width of 0.06 s, sample period of 0.02 s, amplitude of 0.05 V, and pulse period of 0.20 s were applied. X-ray photoelectron spectroscopy (XPS) measurements were performed using a Shimadzu Axis 165 high-performance multi-technique analysis system (Shimadzu, Kyoto, Japan). Spectral data were analyzed using XPSPEAK41 software, and core-level spectra were fitted by considering peak position, intensity, and the minimum number of peaks for the best fit. A Shirley background subtraction was used for fitting all core-level spectra.

2.3. Fabrication of modified electrodes

2.3.1. Preparation of GCE/OD/FMWCNTs modified electrode

The modification procedure for FMWCNTs on GCE is outlined as follows (Scheme 1): First, the well-cleaned GCE was immersed in a 1.0 mM OD solution for 8 h, followed by treatment with a 1:1 mixture of 0.2 mg/mL ethanolic FMWCNTs and 2 mM DCC for 4 h. The amine groups of OD reacted with the carboxyl groups of FMWCNTs in the presence of DCC through a condensation reaction, forming a CO-NH bond and facilitating the attachment of FMWCNTs onto the GCE surface. The resulting electrode was denoted as GCE/OD/FMWCNTs (Rajalakshmi & Abraham John, 2015).

2.3.2. Preparation of GCE/OD/FMWCNTs/p-AMTa modified electrode

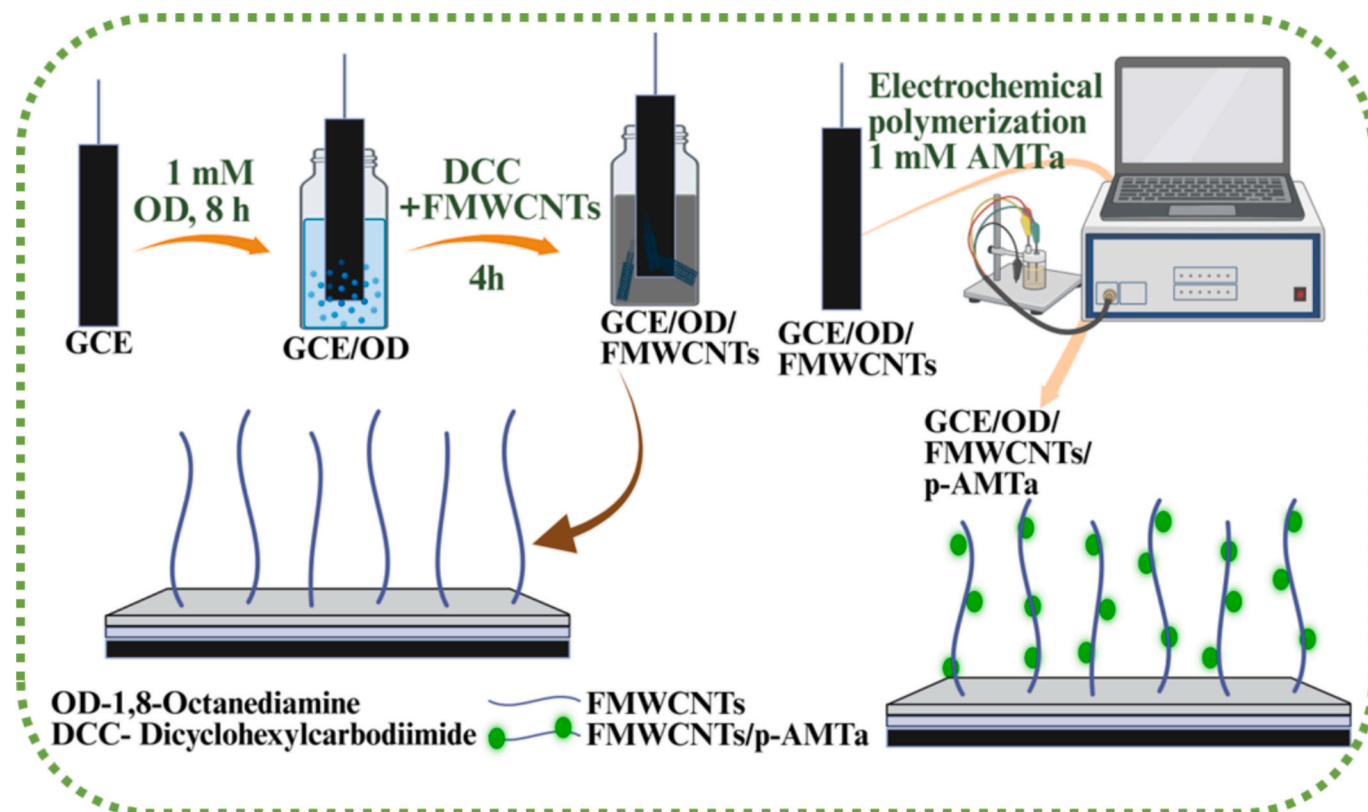
The FMWCNTs/p-AMTa composite was fabricated via potentiodynamic polymerization on the GCE/OD/FMWCNTs modified electrode. A 1 mM AMTa solution in 0.1 M H_2SO_4 was subjected to 15 continuous cycles between -0.2 V and $+1.7$ V at a sweep rate of 50 mV/s (Rajalakshmi et al., 2015).

2.3.3. Preparation of GCE/p-AMTa modified electrode

To evaluate the electrocatalytic activity of the polymer-modified electrode, a GCE/p-AMTa modified electrode was prepared following the procedure described in Section 2.3.2, using a bare GCE instead of the GCE/OD/FMWCNTs modified electrode (Rajalakshmi et al., 2015).

2.4. Sample preparation of real sample analysis

Samples of commercial tea (black tea leaves) and coffee (ground roasted Arabica beans) were purchased from a nearby supermarket in Zhenjiang, Jiangsu, China. Fresh fruit samples, including apples and grapes, were obtained from a local market. The fruits were washed, peeled, blended using a kitchen-grade blender (Midea, Guangdong, China), and dried in a hot air oven at 70 $^{\circ}\text{C}$ for 24 h. Approximately 2.0 g



Scheme 1. Schematic representation of the preparation of FMWCNTs/p-AMTa composite electrode.

of the powdered fruit, coffee, or tea was steeped in 25 mL of distilled water at 80 °C for 10 min for extraction. After filtering, the mixture was centrifuged for 10 min at 5000 rpm. The supernatant was collected, appropriately diluted, and used for electrochemical analysis. The clinical laboratory at the Affiliated People's Hospital of Jiangsu University provided the human blood serum samples, which were anonymized before use. These samples were leftovers from standard diagnostic testing, and no additional blood was drawn specifically for this study. Three blood serum samples were collected from the laboratory, diluted approximately 10 times with PBS, and used for analysis.

3. Results and discussion

3.1. Preparation and characterization of modified electrodes

The electrochemical polymerization of AMTa on the FMWCNTs-modified surface resulted in the appearance of four oxidation peaks at 0.46, 0.76, 1.13, and 1.49 V, and one reduction peak at -0.08 V during the first cycle (Fig. 2). In subsequent cycles, the peaks at 0.76, 1.13, and 1.49 V shifted to 0.69, 0.98, and 1.14 V, respectively, accompanied by a slight decrease in oxidation current response. Additionally, the oxidation peak currents at 1.13 and 1.49 V significantly increased, along with the appearance of a new reduction peak at -0.079 V. These voltammetric behaviors were also observed for the GCE/OD/FMWCNTs, exhibiting higher oxidation and reduction current responses. The enhanced oxidation current responses observed on both electrodes suggest the involvement of a new monomer species in the oxidation process during each potential cycle, leading to an increase in the quantity of electroactive species on the GCE surface (Fig. S1) (Rajalakshmi et al., 2015). The successful attachment of FMWCNTs and the deposition of the nanostructured conducting polymer were confirmed via scanning electron microscopy (SEM) (Fig. 3A, B). The average diameter of the FMWCNTs increased from 38 nm to 45 nm. Atomic force microscopy (AFM) analysis revealed the topology of the modified

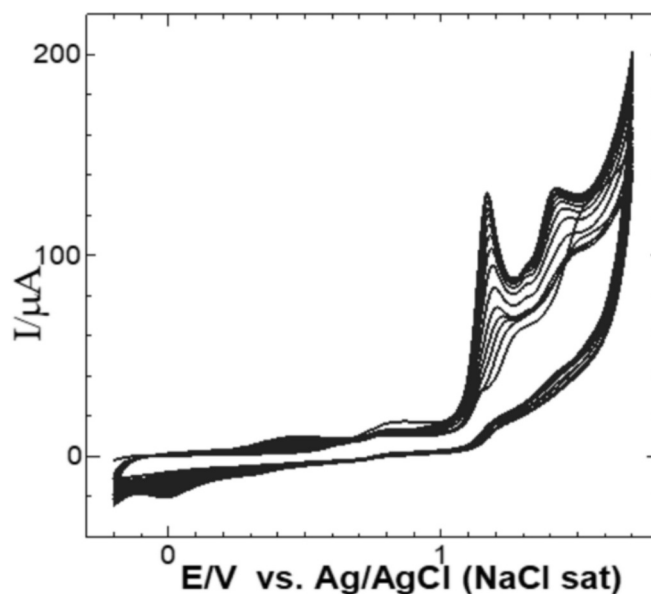


Fig. 2. Electro-polymerization of AMTa at GCE/OD/FMWCNTs in 0.1 M H_2SO_4 + 1 mM AMTa at a sweep rate of 50 mV/s.

surfaces. The FMWCNTs-modified surface exhibited aligned, fibrous, and tubular features, characteristic of well-dispersed FMWCNTs, indicating the successful deposition of FMWCNTs on the GCE surface (Fig. S2A). After incorporating p-AMTa, the AFM image showed a more compact and smoother morphology, with the nanotube network partially embedded in the polymer matrix. The rounded, dense features indicated uniform polymer growth over the FMWCNTs network, which likely contributed to improved electrochemical stability and enhanced

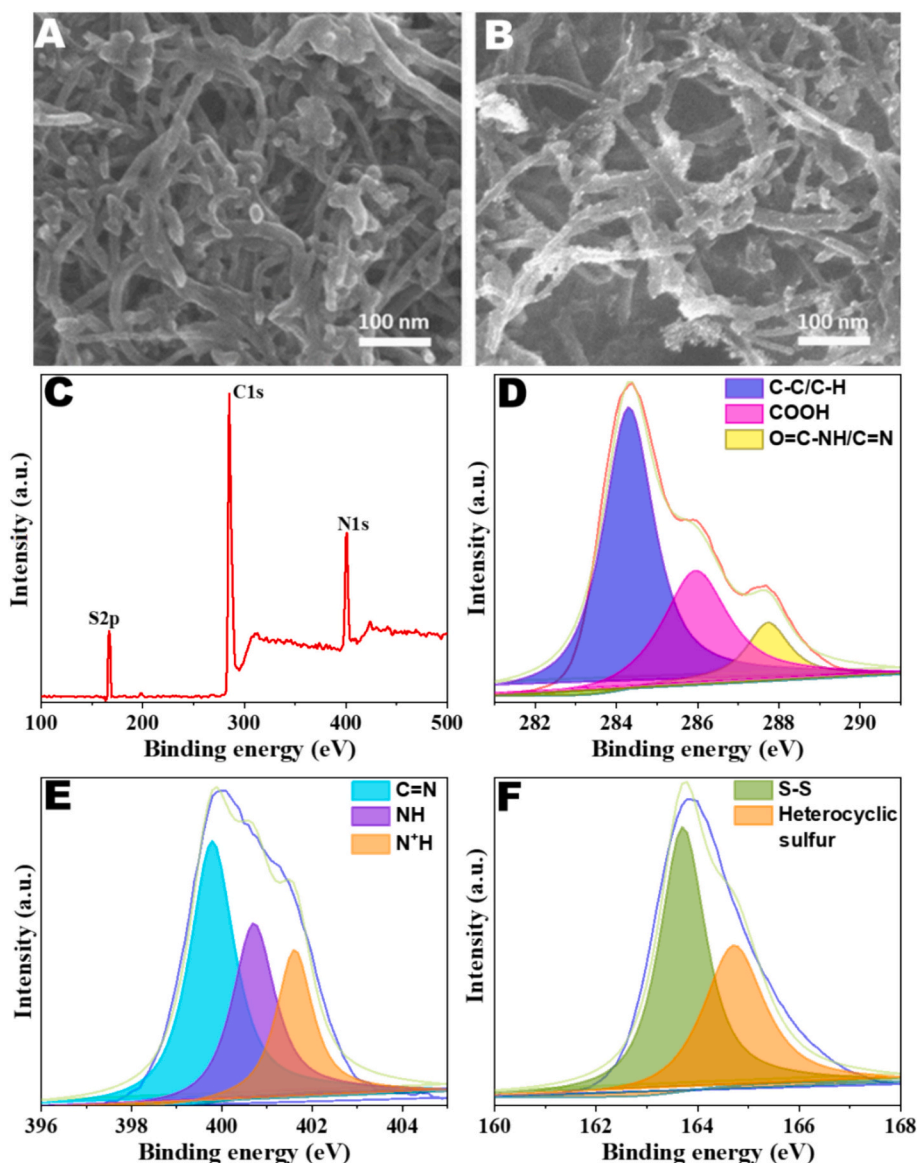


Fig. 3. SEM images obtained for (A) GCE/OD/FMWCNTs and (B) GCE/OD/FMWCNTs/p-AMTa composite modified surfaces. XPS (C) wide scan, (D) C1s, (E) N1s and (F) S2p regions of GCE/OD/FMWCNTs/p-AMTa surfaces.

surface functionalization (Fig. S2B). These topographical changes confirm the successful formation of the composite and support the improved electrochemical performance observed in the voltammetric studies. Additionally, the bonding nature was investigated using XPS analysis (Fig. 3C–3F). The survey spectrum revealed that the composite-modified surface contained carbon (C), nitrogen (N), and sulfur (S) species (Fig. 3C). The C1s spectrum was deconvoluted into three peaks at 284.3, 287.8, and 286.3 eV, which were attributed to C-C/C-H, O=C-NH-, and C—O— species, respectively. The core-level spectrum of N1s from the composite-modified surface (Fig. 3D) was fitted with three component peaks at 399.8, 400.7, and 401.6 eV, corresponding to -N=, -NH-, and -N + H-, respectively (Fig. 3E). In the sulfur core-level spectrum, S—S and heterocyclic sulfur sulfate ion peaks were observed at 163.6 and 164.9 eV (Fig. 3F). The peak at 287.8 eV in the carbon core-level spectrum was attributed to the amide bond formation between FMWCNTs and the OD linker on the GCE surface. Furthermore, the formation of the -C=N bond during polymerization was confirmed by the peak observed at 399.8 eV in the nitrogen-deconvoluted spectrum. These results are consistent with those reported in the literature (Rajalakshmi et al., 2015).

3.2. Electro-oxidation of 3-CQA at different modified electrodes

The electro-oxidation of 3-CQA was investigated using unmodified GCE, GCE/p-AMTa, GCE/OD/FMWCNTs, and GCE/OD/FMWCNTs/p-AMTa electrodes in 0.2 M PBS containing 0.5 mM 3-CQA (pH 7.2) at a sweep rate of 50 mV/s (Fig. 4). The unmodified GCE displayed oxidation and reduction responses at 0.27 V and 0.14 V (curve a), as illustrated in Scheme 2A. The electrochemical oxidation of 3-CQA results in the formation of its o-quinone, which is then reduced back to 3-CQA, involving two electrons and two protons (Yardim, 2012). However, after five consecutive cycles, the redox responses shifted to 0.31 V and 0.12 V with reduced current responses (Fig. S3, dashed line-a). This behavior is attributed to the passivation of the GCE surface by the oxidized compounds of 3-CQA, making the unmodified GCE unsuitable for 3-CQA detection. In contrast, the GCE/p-AMTa electrode exhibited significantly improved redox responses (2.1 times higher than the unmodified GCE), with oxidation and reduction peaks at 0.26 V and 0.12 V, respectively (curve b).

The enhanced electro-oxidation response on GCE/p-AMTa (Scheme 2B) is primarily attributed to hydrogen bonding and electrostatic

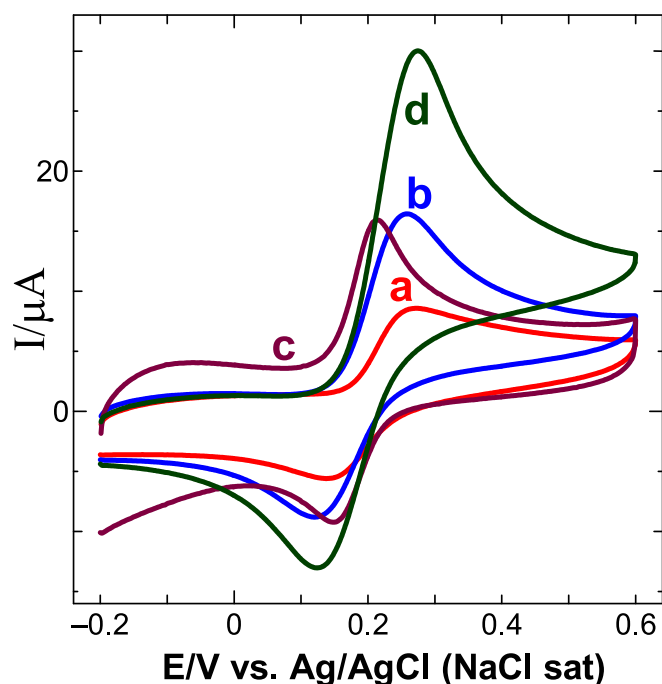
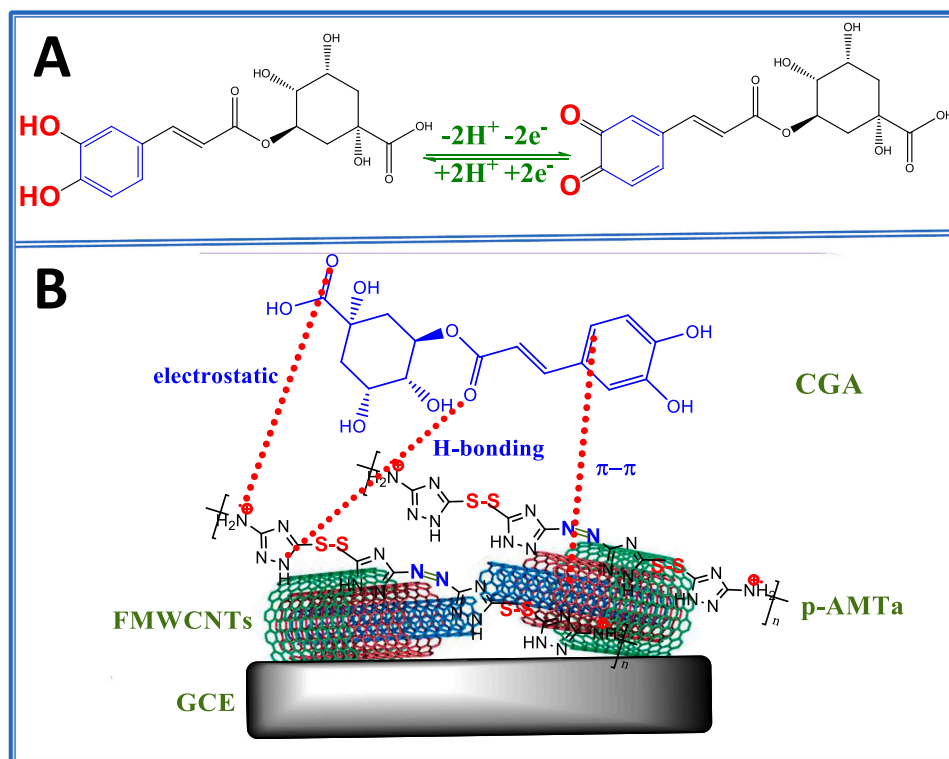


Fig. 4. CVs obtained for (a) unmodified GCE, (b) GCE/p-AMTa, (c) GCE/OD/FMWCNTs and (d) GCE/OD/FMWCNTs/p-AMTa in 0.2 M PBS + 0.5 mM of 3-CQA at a sweep rate of 50 mV/s.

interactions between the heteroatoms of p-AMTa and 3-CQA. These redox responses remained stable over five cycles on the GCE/p-AMTa electrode (Fig. S3, dashed line-b). Further improvement was observed upon the introduction of GCE/OD/FMWCNTs, where the oxidation response shifted to 0.21 V and the reduction response was observed at

0.15 V (curve c). The 59 mV shift in potential and similar oxidation current responses to GCE/p-AMTa, along with stable redox responses after five cycles (Fig. S3, dashed line-c), can be attributed to the π - π interactions between FMWCNTs and the benzene ring of 3-CQA (Scheme 2B). Interestingly, the GCE/OD/FMWCNTs/p-AMTa electrode demonstrated a significantly enhanced redox response at 0.27 V and 0.12 V, along with a fourfold increase in electro-oxidation current compared to the unmodified GCE (curve d). The oxidation and reduction peaks of 3-CQA remained highly stable during successive scans, as shown in Fig. S3 (dashed line-d). The superior sensitivity of this composite electrode is mainly attributed to the strong electrostatic and hydrogen bonding interactions between the heteroatoms on the positively charged polymer backbone and the π - π interactions between the FMWCNTs and the aromatic ring of 3-CQA (Scheme 2B). The cyclic voltammetry (CV) profiles (Fig. S1; Curve 'd') demonstrate that the current response remained stable and reproducible over successive scans, with no significant loss in peak intensity or shift in redox potential, indicating excellent surface anti-fouling properties. The enhanced electrocatalytic performance of the FMWCNTs/p-AMTa electrode can be attributed to several factors: the large surface area and π - π interaction capabilities of the MWCNTs, which prevent analyte accumulation on the surface; the hydrophilic and positively charged p-AMTa polymer, which maintains a clean, electro-active surface through favorable electrostatic and hydrogen bonding interactions with 3-CQA; and the synergistic composite layer architecture that discourages the deposition of oxidation products while enhancing mass transport. These combined properties reduce electrode passivation, ensuring stable antifouling behavior, making this system highly suitable for real-sample analysis in complex matrices such as food and biological fluid.

The chemical interactions and contributions of functional groups were further analyzed using FT-IR spectra (Fig. S4). The composite film exhibited an absorption band around 3200–3400 cm^{-1} , corresponding to the N—H and O—H stretching vibrations, indicative of the presence of primary amine and hydroxyl groups. Peaks near 1650 cm^{-1} were



Scheme 2. (A) Proposed electro-oxidation mechanism of 3-CQA, where the catechol undergoes reversible redox process forming o-quinone intermediate. (B) Schematic representation of the electrostatic, hydrogen bonding and π - π stacking interaction between 3-CQA and FMWCNTs/p-AMTa interface.

attributed to the C=N stretching vibrations of the triazole ring. A peak around 2550–2600 cm^{-1} corresponded to S–H stretching, characteristic of the thiol group present in AMTa. Upon interaction with 3-CQA, the –OH/N–H band broadened and slightly shifted, suggesting hydrogen bonding interactions between the hydroxyl/amine groups on the composite surface and the functional groups of 3-CQA. The C=N stretching band remained intact, though it may have undergone minor shifts or changes in intensity, indicating electrostatic interactions or environmental changes around the triazole ring due to composite formation. Additionally, enhanced intensity in the C=C stretching region (around 1500–1600 cm^{-1}) suggests π – π stacking interactions between the conjugated structures of FMWCNTs and 3-CQA. These spectral changes confirm the presence of hydrogen bonding, electrostatic interactions, and π – π stacking, all contributing to the improved electrochemical properties of the modified electrode.

The effect of scan rates on the GCE/OD/FMWCNTs/p-AMTa electrode was investigated in relation to the oxidation of 3-CQA (Fig. S5). A good linear relationship was observed between anodic peak currents and the square root of the scan rates, with an R^2 of 0.9980 (Inset: Fig. S5), indicating that the oxidation of 3-CQA was predominantly a diffusion-controlled process on the composite electrode.

3.3. Effect of solution pH

The pH effect on the redox reaction of 3-CQA was also studied under similar experimental conditions. The CV results for 3-CQA in the pH range from 3 to 10 in 0.2 M PBS and the corresponding plot of pH vs. oxidation potential are shown in Fig. S6. Both the peak potential and peak current were pH-dependent. As the pH increased from 3 to 10, the redox peaks shifted gradually toward the lower potential window. The anodic peak potential of 3-CQA varied linearly with pH, with a slope of 36 mV per pH. This result aligns with previous reports suggesting that two protons and two electrons participate in the 3-CQA redox process (Salimi et al., 2005). Additionally, the oxidation current of 3-CQA reached its maximum at pH 7. Given the optimal conditions, which offer superior stability, reproducibility, and biocompatibility for real sample analysis, pH 7.2 was chosen for further studies.

3.4. Determination of 3-CQA by DPV

The DPV profiles for 3-CQA were obtained over a concentration range of 1 to 11 μM at the GCE/OD/FMWCNTs/p-AMTa electrode in 0.2 M PBS (pH 7.2). Introduction of 1 μM 3-CQA resulted in a peak at 0.17 V (Fig. 5A; curve a). As the concentration of 3-CQA was increased by

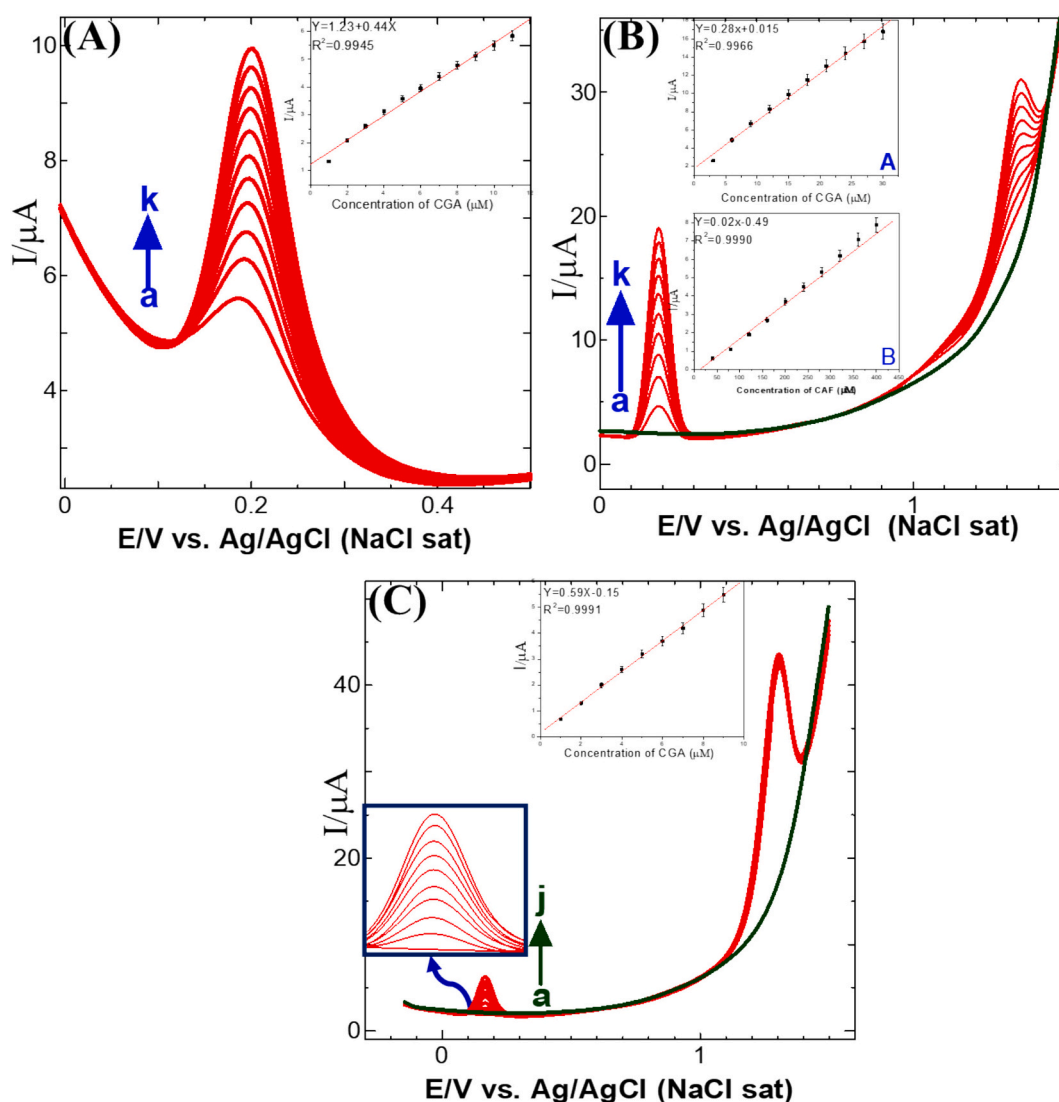


Fig. 5. DPVs obtained for the detection of 3-CQA at GCE/OD/FMWCNTs/p-AMTa in 0.2 M PBS (A) each addition of 1 μM of 3-CQA (1–11 μM ; a–k), (B) each addition of 3 μM 3-CQA and 40 μM CAF and (C) each addition of 1 μM of 3-CQA in AMTa in 0.2 M PBS + 500 μM CAF. **Insets:** Corresponding Linear plots derived from current vs. concentration of 3-CQA.

successive 1 μM increments up to 11 μM , the oxidation current response exhibited a dynamic increase (curves b–k), demonstrating a linear relationship with an R^2 of 0.9945 (Inset: Fig. 5A). The oxidation peak potential for 3-CQA remained almost constant despite the increase in concentration up to 11 μM .

3.5. Detection of 3-CQA along with CAF

Given that 3-CQA naturally occurs in coffee beans alongside CAF, simultaneous detection of both is critical. Fig. 5B presents the DPVs for various concentrations of 3-CQA and CAF. The addition of 3 μM 3-CQA and 40 μM CAF resulted in distinct oxidation peaks at 0.19 V and 1.34 V, corresponding to 3-CQA and CAF, respectively (curve b). Both catalytic responses were progressively enhanced, with R^2 values of 0.9966 and 0.9990 for 3-CQA and CAF, respectively, as the concentrations of 3-CQA increased from 3 to 30 μM and CAF from 40 to 400 μM (curves b–k).

3.6. Specific detection of 3-CQA along with CAF

The selectivity of the GCE/OD/FMWNTs/p-AMTa electrode for 3-CQA detection in the presence of excess CAF was also evaluated. Given the abundant presence of CAF with 3-CQA in natural sources such as coffee, selective determination of 3-CQA in the presence of high CAF concentrations is crucial. Fig. 5C shows the DPVs recorded after adding 1 μM 3-CQA and 0.5 mM CAF in 0.2 M PBS. A distinguishable oxidation response was observed at 0.17 V for 1 μM 3-CQA even in the presence of 0.5 mM CAF, as shown in Fig. 5C (curve b), demonstrating the ability to detect low concentrations of 3-CQA in the presence of 500-fold excess CAF. As the concentration of 3-CQA increased from 1 to 9 μM , its oxidation current response gradually improved, with an R^2 of 0.9991 for each successive addition of 1 μM 3-CQA in 0.2 M PBS (pH 7.2) + 0.5 mM CAF.

3.7. Amperometric detection of 3-CQA

Fig. 6 presents the chronoamperometric *i*-t profile for 3-CQA detection using the FMWNTs/p-AMTa composite electrode in a homogeneously stirred 0.2 M PBS at a constant working potential of +0.4 V. The initial amperometric current profile (1200 s) reflects the addition of 100 nM 3-CQA (Fig. 6A). Subsequent additions of 100 nM 3-CQA at 50-s intervals resulted in a stepwise increase in the amperometric current, with the current stabilizing within 3 s after each injection. The current

response as a function of successive 3-CQA additions (ranging from 100 to 1000 nM) showed a highly linear relationship, with an R^2 of 0.9998 (Inset: Fig. 6A).

Additionally, the chronoamperometric response improved progressively with increasing concentrations of 3-CQA, from 0.1 to 200 μM (Fig. 6B), yielding a correlation coefficient of 0.9998. The corresponding correlation plot and expanded view are shown in the inset of Fig. 6B, with an LOD for 3-CQA reaching as low as 30 nM ($S/N = 3$). Furthermore, the electrode fabrication process was simple and efficient compared to previously reported sensors, as detailed in Table S1. The FMWNTs/p-AMTa composite electrode demonstrated an exceptionally broad linear range (0.1–200 μM) and the lowest LOD (30 nM) among the listed sensors. For instance, the nanogold-modified electrode, which exhibited an LOD of 40 nM, had a narrow linear range (0.01–0.1 μM), limiting its broader applicability (Chauhan & Annu, 2020). In contrast, the metal complex-modified carbon paste electrode had a higher detection limit and a restricted linear range (80.2–800 nM) (de Carvalho et al., 2008). Additionally, tyrosine-modified sensors faced issues with enzyme instability and higher LODs (1400 nM) (Munteanu & Apetrei, 2022). The superior sensing performance of the proposed electrode arises from the synergistic effects of FMWNTs and the p-AMTa layer. This method offers a robust, cost-effective, and scalable alternative to existing techniques for electrochemical 3-CQA detection, making it particularly promising for practical applications in food safety monitoring and clinical diagnostics.

3.8. Effect of interferences

3-CQA was also detected in the presence of various co-interferents, including cysteine, citrate, guanosine monophosphate, alanine, asparagine, thymine, and tryptophan. Fig. 7 displays the chronoamperometric *i*-t profile of 3-CQA at the FMWNTs/p-AMTa composite electrode surface in consistently stirred 0.2 M PBS. The initial enhancement of the amperometric current signal at 1300 s resulted from the addition of 200 nM of 3-CQA (curve “a” in Fig. 7). Subsequent injections of 3-CQA produced a distinct current response at 1350 s. Notably, no significant amperometric current responses were observed when 100 μM each of cysteine, citrate, alanine, guanosine monophosphate, asparagine, tryptophan, and thymine were added to the solution (Fig. 7, curves b–h). However, an additional 200 nM of 3-CQA introduced into this solution led to a noticeable increase in the amperometric current at 1750 s, mirroring the initial response at 1300 s (curve “a”). These results

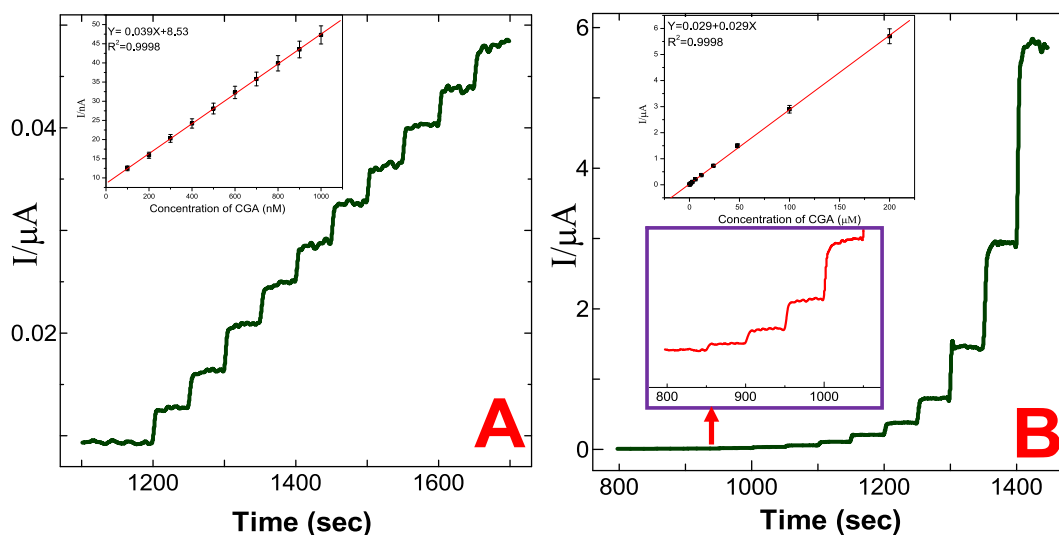


Fig. 6. Chronoamperometric *i*-t profile obtained for the detection of 3-CQA at GCE/OD/FMWNTs/p-AMTa in 0.2 M PBS. (A) The addition of 3-CQA was about 100 nM at 50 s intervals. (B) The injection of 3-CQA by 0.1, 0.2, 0.4, 0.8, 1.5, 3, 6, 15, 30, 50, 100 and 200 μM at 50 s intervals. $E_{\text{app}} = +0.4$ V. **Insets:** Respective linear plots and expanded views.

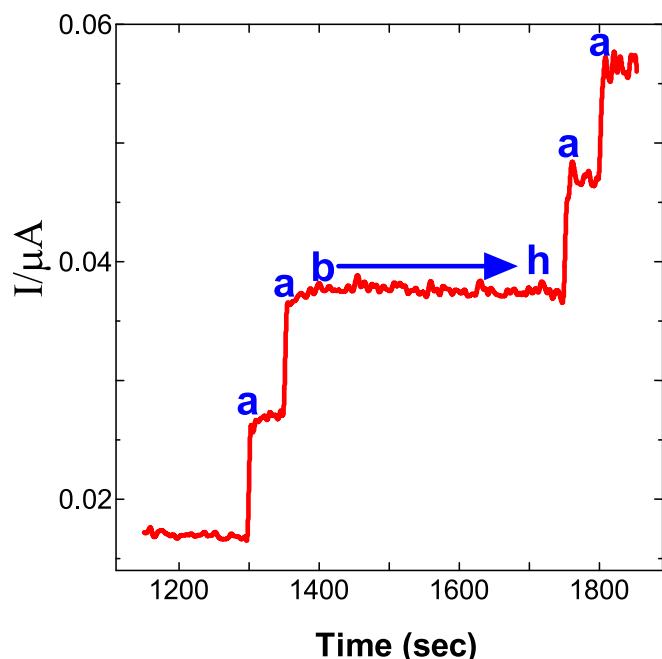


Fig. 7. Chronoamperometric *i-t* profile obtained at GCE/OD/FMWCNTs/p-AMTa in 0.2 M PBS + (a) 200 nM 3-CQA and addition of 100 μ M each (b) cysteine, (c) citrate, (d) alanine, (e) guanosine monophosphate, (f) asparagine, (g) tryptophan, and (h) thymine. $E_{app} = +0.4$ V.

confirm that 200 nM 3-CQA can be reliably detected even in the presence of a 500-fold excess of key interfering compounds. Further chronoamperometric measurements were conducted to evaluate the selectivity of the GCE/OD/FMWCNTs/p-AMTa electrode for 3-CQA detection. As shown in Fig. S4, the sensor displayed minimal current changes upon the addition of various potentially interfering species (100 μ M of cysteine, citrate, alanine, GMP, asparagine, tryptophan, and thymine), while a significant increase in current was observed upon the addition of just 400 nM 3-CQA. This demonstrates the electrode's high selectivity for 3-CQA, even in the presence of excess biomolecules and electroactive species. The chronoamperometric response further validates the practical applicability of this sensor for selectively detecting 3-CQA in complex sample matrices.

3.9. Real sample analysis

The practical performance of the FMWCNTs/p-AMTa composite surface was demonstrated by detecting trace levels of 3-CQA in blood serum, coffee bean extracts, tea extracts, potatoes, tomatoes, apples, and grapes. Fig. S8 shows the DPVs for coffee bean extract, both alone and spiked with commercial 3-CQA and CAF. PBS showed no electrochemical response (curve a). In contrast, the coffee bean extract in PBS exhibited peaks at 0.19 V and 1.34 V (curve b). After spiking with commercial 3-CQA and CAF, the peak currents increased at these same potentials. Based on the oxidation current of 3-CQA, the concentration of 3-CQA in the coffee bean extract was calculated. The actual and projected amounts of 3-CQA are presented in Table S2, demonstrating good recoveries of 3-CQA in the coffee bean extract and highlighting the potential of the proposed composite for detecting 3-CQA in real food samples. Similarly, other food samples were tested by adding a known amount of 3-CQA, and the added and found amounts of 3-CQA are summarized in Table S2, showing good recovery results across all biological and food samples.

3.10. Repeatability, reproducibility, and stability of FMWCNTs/p-AMTa composite

An experiment was conducted to assess both the repeatability (intra-assay precision) and reproducibility (inter-assay precision) of the developed biosensor at three 3-CQA concentration levels: low (0.1 μ M), medium (100 μ M), and high (200 μ M) (Fig. S9). For repeatability, ten independent measurements were made using the same biosensor under identical conditions. For reproducibility, measurements were performed using independently fabricated biosensors ($n = 10$) at each concentration level. The relative standard deviations (RSDs) for both sets of experiments were calculated and presented in Fig. S6. The consistently low RSD values across all concentrations confirm the high precision and reliability of the biosensor for quantitative analysis of 3-CQA.

The stability of the modified electrode was evaluated in the presence of 0.2 mM 3-CQA in 0.2 M PBS. CVs were recorded for 3-CQA in 0.2 M PBS over a 10-min period, showing that the oxidation response of 3-CQA maintained nearly identical features, with an RSD of 1.5 % over at least four successive analyses. Additionally, after two weeks of storage at 4 °C in an argon chamber, the oxidation response of 3-CQA decreased by only 1.1 %. To assess reusability, three independent GCE/OD/FMWCNTs/p-AMTa surfaces were prepared and tested for the oxidation of 3-CQA over six repeated measurements. The catalytic peak currents for these six repeated experiments remained closely identical, with an RSD of 2.23 %, demonstrating significant reproducibility.

4. Conclusions

Sensitive detection of 3-CQA was demonstrated using the FMWCNTs/p-AMTa composite electrode at physiological pH. The electrode exhibited a stable response with a fourfold increase in oxidation current response to 3-CQA, primarily attributed to the hydrogen bonding and electrostatic interactions between the heteroatoms on the positively charged polymer backbone and 3-CQA, as well as the π - π interactions between FMWCNTs and the benzene ring of 3-CQA. The chronoamperometric current response was highly responsive to varying concentrations of 3-CQA, from 0.1 to 200 μ M, with an LOD of 30 nM ($S/N = 3$). Furthermore, the FMWCNTs/p-AMTa composite electrode demonstrated good recovery for 3-CQA in biological and food samples. This work suggests that the proposed sensor is a promising platform for detecting the phenolic antioxidant 3-CQA in food and biological samples. Additionally, integrating this sensor into portable or wearable electrochemical devices could enable on-site analysis and rapid detection. Future efforts may focus on improving sensor stability over time and under varying conditions and developing multiplexed detection systems for food quality and health monitoring.

CRedit authorship contribution statement

Hao Tang: Data curation, Conceptualization. **Jian Shen:** Formal analysis, Data curation. **Jindong Dai:** Investigation. **Kanagaraj Rajalakshmi:** Writing – original draft, Investigation, Formal analysis. **Selvaraj Muthusamy:** Writing – review & editing, Methodology, Investigation, Conceptualization. **Palanisamy Kannan:** Writing – review & editing, Methodology, Investigation. **Dongwei Zhu:** Writing – review & editing, Supervision, Funding acquisition. **Benshuai You:** Writing – original draft, Supervision. **Xiaojuan Liu:** Writing – review & editing, Funding acquisition.

Declaration of competing interest

The authors declare that they have no known competing financial interests or personal relationships that could have appeared to influence the work reported in this paper.

Acknowledgements

The authors thanks to Jinshan Elite Talents in the Medical Field (JSYC2023-008), Project of Jiangsu Provincial Administration of Traditional Chinese Medicine (MS2023144), Project of Zhenjiang Science and Technology Bureau (SH2023066), National Natural Science Foundation of China (82402487), Natural Science Foundation of Jiangsu Province (BK20240512) and Bullet edits limits for the linguistic editing and proofreading of the manuscript.

Appendix A. Supplementary data

Supplementary data to this article can be found online at <https://doi.org/10.1016/j.foodchem.2025.145337>.

Data availability

No data was used for the research described in the article.

References

- Agar, O. T., Dikmen, M., Ozturk, N., Yilmaz, M. A., Temel, H., & Turkmenoglu, F. P. (2015). Comparative studies on phenolic composition, antioxidant, wound healing and cytotoxic activities of selected Achillea L. *Species Growing in Turkey, Molecules*, 20(10), 17976–18000. <https://www.mdpi.com/1420-3049/20/10/17976>.
- Alagumalai, K., Shanmugam, R., Chen, S.-M., Arumugam, B., Chen, T.-W., Yu, J., Liu, X., & Kannan Ramaraj, S. (2022). A portable advanced electrocatalyst for polyphenolic 3-Caffeoylquinic acid evaluation in food samples. *Chemical Engineering Journal*, 435, Article 134796. <https://www.sciencedirect.com/science/article/abs/pii/S1385894722003035>.
- de Carvalho, M. L., Santhiago, M., Peralta, R. A., Neves, A., Micke, G. A., & Vieira, I. C. (2008). Determination of 3-Caffeoylquinic acid in coffee using a biomimetic sensor based on a new tetranuclear copper(II) complex. *Talanta*, 77(1), 394–399. <https://pubmed.ncbi.nlm.nih.gov/18804651/>.
- Chauhan, P., Annu Raja, A. N., & Jain, R. (2020). Nanogold modified glassy carbon sensor for the quantification of phytoestrogen 3-Caffeoylquinic acid. *Surfaces and Interfaces*, 19, Article 100536. <https://www.sciencedirect.com/science/article/abs/pii/S2468023019307278>.
- Chen, X., Mao, J., Wen, F., & Xu, X. (2021). Determination of phenolic acids in botanical pharmaceutical products by capillary electrophoresis with Chemiluminescence detection. *Analytical Letters*, 54(5), 817–829. <https://doi.org/10.1080/00032719.2020.1783675>.
- Cho, A.-S., Jeon, S.-M., Kim, M.-J., Yeo, J., Seo, K.-I., Choi, M.-S., & Lee, M.-K. (2010). 3-Caffeoylquinic acid exhibits anti-obesity property and improves lipid metabolism in high-fat diet-induced-obese mice. *Food and Chemical Toxicology*, 48(3), 937–943. <https://pubmed.ncbi.nlm.nih.gov/20064576/>.
- Clifford, M. N. (1999). 3-Caffeoylquinic acid s and other cinnamates – Nature, occurrence and dietary burden. *Journal of the Science of Food and Agriculture*, 79(3), 362–372. [https://scijournals.onlinelibrary.wiley.com/doi/abs/10.1002/\(SICI\)1097-0010\(20000515\)80:7%3C1033::AID-JSFA595%3E3.0.CO;2-T](https://scijournals.onlinelibrary.wiley.com/doi/abs/10.1002/(SICI)1097-0010(20000515)80:7%3C1033::AID-JSFA595%3E3.0.CO;2-T).
- Duthie, S. J., Johnson, W., & Dobson, V. L. (1997). The effect of dietary flavonoids on DNA damage (strand breaks and oxidised pyrimidines) and growth in human cells. *Mutation Research/Genetic Toxicology and Environmental Mutagenesis*, 390(1), 141–151. <https://pubmed.ncbi.nlm.nih.gov/9150762/>.
- Gigl, M., Frank, O., Irmer, L., & Hofmann, T. (2022). Identification and quantitation of reaction products from 3-Caffeoylquinic acid, Caffeic acid, and their thermal degradation products with odor-active thiols in coffee beverages. *Journal of Agricultural and Food Chemistry*, 70(17), 5427–5437. <https://pubmed.ncbi.nlm.nih.gov/35467336/>.
- Kasai, H., Fukada, S., Yamaizumi, Z., Sugie, S., & Mori, H. (2000). Action of 3-Caffeoylquinic acid in vegetables and fruits as an inhibitor of 8-hydroxydeoxyguanosine formation in vitro and in a rat carcinogenesis model. *Food and Chemical Toxicology*, 38(5), 467–471. <https://pubmed.ncbi.nlm.nih.gov/10762733/>.
- Krizman, M., Baricevic, D., & Prosek, M. (2007). Determination of phenolic compounds in fennel by HPLC and HPLC–MS using a monolithic reversed-phase column. *Journal of Pharmaceutical and Biomedical Analysis*, 43(2), 481–485. <https://www.sciencedirect.com/science/article/abs/pii/S073170850600478X>.
- Mariyappan, V., Chen, S.-M., Jeyapragasam, T., & Devi, J. M. (2022). Designing and construction of a cobalt-metal-organic framework/heteroatoms co-doped reduced graphene oxide mesoporous nanocomposite based efficient electrocatalyst for 3-Caffeoylquinic acid detection. *Journal of Alloys and Compounds*, 898, Article 163028. <https://www.sciencedirect.com/science/article/abs/pii/S0925838821044388>.
- Munteanu, I. G., & Apetrei, C. (2021). A review on electrochemical sensors and biosensors used in 3-Caffeoylquinic acid Electroanalysis. *International Journal of Molecular Sciences*, 22(23), 13138. <https://pmc.ncbi.nlm.nih.gov/articles/PM/C8658152/>.
- Munteanu, I. G., & Apetrei, C. (2022). Tyrosinase-based biosensor—A new tool for 3-Caffeoylquinic acid detection in nutraceutical formulations. *Materials*, 15(9), 3221. <https://pubmed.ncbi.nlm.nih.gov/35591555/>.
- Olthof, M. R., Hollman, P. C. H., & Katan, M. B. (2001). 3-Caffeoylquinic acid and Caffeic acid are absorbed in humans. *The Journal of Nutrition*, 131(1), 66–71. <https://www.sciencedirect.com/science/article/pii/S0022316622144597>.
- Rajalakshmi, K., & Abraham John, S. (2015). Chemical attachment of functionalized multiwalled carbon nanotubes on glassy carbon electrode for electrocatalytic application. *Electrochimica Acta*, 165, 268–276. <https://www.sciencedirect.com/science/article/abs/pii/S0013468615001280>.
- Salimi, A., Hallaj, R., & Ghadermazi, M. (2005). Modification of carbon ceramic electrode prepared with sol–gel technique by a thin film of 3-Caffeoylquinic acid: Application to amperometric detection of NADH. *Talanta*, 65(4), 888–894. <https://pubmed.ncbi.nlm.nih.gov/18969884/>.
- de Souza Farias, S. A., da Costa, K. S., & Martins, J. B. L. (2021). Analysis of conformational, structural, magnetic, and electronic properties related to antioxidant activity: Revisiting Flavon, Anthocyanidin, flavanone, Flavonol, Isoflavone, flavone, and Flavan-3-ol. *ACS Omega*, 6(13), 8908–8918. <https://doi.org/10.1021/acsomega.0c06156>.
- Tajik, N., Tajik, M., Mack, I., & Enck, P. (2017). The potential effects of 3-Caffeoylquinic acid, the main phenolic components in coffee, on health: A comprehensive review of the literature. *European Journal of Nutrition*, 56(7), 2215–2244. <https://pubmed.ncbi.nlm.nih.gov/28391515/>.
- Tong, C., Shi, F., Tong, X., Shi, S., Ali, G., & I. Y. (2021). Shining natural flavonols in sensing and bioimaging. *TrAC Trends in Analytical Chemistry*, 137, Article 116222. <https://www.sciencedirect.com/science/article/abs/pii/S0165993621000443>.
- Umapathi, R., Raju, C. V., Safarkhani, M., Haribabu, J., Lee, H. U., Rani, G. M., & Huh, Y. S. (2025). Versatility of MXene based materials for the electrochemical detection of phenolic contaminants. *Coordination Chemistry Reviews*, 525, Article 216305 (<https://www.sciencedirect.com/science/article/abs/pii/S0010854524006519>).
- Umapathi, R., Rethinasabapathy, M., Kakani, V., Kim, H., Park, Y., Kim, H. K., Rani, G. M., Kim, H., & Huh, Y. S. (2025). Hexagonal boron nitride composite film based triboelectric nanogenerator for energy harvesting and machine learning assisted handwriting recognition. *Nano Energy*, 136, Article 110689. <https://www.sciencedirect.com/science/article/abs/pii/S2211285525000485>.
- Xie, W., Yu, Y., Hou, M., Zhang, Y., Yu, H., Zhang, H., Zhang, G., & G., Jing, H., & Chen, A. (2022). Simultaneous separation and determination of five 3-Caffeoylquinic acid isomers in honeysuckle by capillary electrophoresis using self-synthesized ionic liquid [N-methylimidazole- β -cyclodextrin] [bromide] as separation selector. *Journal of Separation Science*, 45(16), 3197–3207. <https://pubmed.ncbi.nlm.nih.gov/35772030/>.
- Yang, Z.-S., Long, H.-Y., Zhang, X.-Y., & Wang, Y. (2008). Autooxidative activity of 3-Caffeoylquinic acid and damage to DNA. *Electroanalysis*, 20(18), 1968–1972. <https://doi.org/10.1002/elan.200804271>.
- Yardim, Y. (2012). Electrochemical behavior of 3-Caffeoylquinic acid at a boron-doped diamond electrode and estimation of the antioxidant capacity in the coffee samples based on its oxidation peak. *Journal of Food Science*, 77(4), C408–C413. <https://pubmed.ncbi.nlm.nih.gov/22394181/>.
- Zhang, X., Huang, H., Yang, T., Ye, Y., Shan, J., Yin, Z., & Luo, L. (2010). 3-Caffeoylquinic acid protects mice against lipopolysaccharide-induced acute lung injury. *Injury*, 41(7), 746–752. <https://pubmed.ncbi.nlm.nih.gov/20227691/>.
- Zhang, Y., Cao, C., Yang, Z., Jia, G., Liu, X., Li, X., Cui, Z., & Li, A. (2023). Simultaneous determination of 20 phenolic compounds in propolis by HPLC-UV and HPLC-MS/MS. *Journal of Food Composition and Analysis*, 115, Article 104877. <https://www.sciencedirect.com/science/article/abs/pii/S0889157522004951>.
- Zheng, L.-F., Dai, F., Zhou, B., Yang, L., & Liu, Z.-L. (2008). Prooxidant activity of hydroxycinnamic acids on DNA damage in the presence of Cu(II) ions: Mechanism and structure–activity relationship. *Food and Chemical Toxicology*, 46(1), 149–156. <https://pubmed.ncbi.nlm.nih.gov/17764801/>.